Impact of ligands on structural and optical properties of Ag_{29} nanoclusters

Yuan Zeng,[1] Shana Havenridge,[2] Mustafa Gharib,[1,3] Ananya Baksi,[4] K. L. Dimuthu M. Weerawardene,[2,5] Anna Rosa Ziefuß,[6] Christian Strelow,[7] Christoph Rehbock,[6] Alf Mews,[7] Stephan Barcikowski,[6] Manfred M. Kappes,[4] Wolfgang J. Parak,[1,7,8*] Christine M. Aikens,[2*] Indranath Chakraborty[1*]

[1]Department of Physics and Center for Hybrid Nanostructure (CHyN), University of Hamburg, Luruper Chaussee 149, Hamburg 22761, Hamburg, Germany

[2] Department of Chemistry, Kansas State University, Manhattan, Kansas 66506, United States

[3] Radiation Biology Department, Egyptian Atomic Energy Authority (EAEA), Cairo, Egypt

[4] Institute of Nanotechnology, Karlsruhe Institute of Technology, 76344 Eggenstein-Leopoldshafen, Germany

[5] Department of Chemistry, Baylor University, Waco, TX, 76798, United States

[6]Department of Technical Chemistry I, University of Duisburg-Essen and Center for Nanointegration Duisburg-Essen (CENIDE), Essen, Germany

[7]Department of Chemistry, University of Hamburg, Grindelallee 117, 20146 Hamburg, Germany

[8]CIC Biomagune, San Sebastian, Spain

KEYWORDS. Silver nanoclusters, ligands, ion mobility mass spectrometry, photoluminescence, structure-property

ABSTRACT: A ligand exchange strategy has been employed to understand the role of ligands on the structural, and optical properties of atomically precise 29 atom silver nanoclusters (NCs). By ligand optimization, ~ 44-fold quantum yield (QY) enhancement of $Ag_{29}(BDT)_{12-x}(DHLA)_x$ NCs (x = 1-6) was achieved, where BDT and DHLA refer to 1,3-benzene-dithiol and dihydrolipoic acid, respectively. High-resolution mass spectrometry was used to monitor ligand exchange, and structures of the different NCs were obtained through density functional theory (DFT). The DFT results from $Ag_{29}(BDT)_{11}(DHLA)$ NCs were further experimentally verified through collisional cross-section (CCS) analysis using ion mobility mass spectrometry (IM MS). An excellent match in predicted CCS values and optical properties with the respective experimental data lead to a likely structure of $Ag_{29}(DHLA)_{12}$ NCs consisting of an icosahedral core with an $Ag_{16}S_{24}$ shell. Combining the experimental observation with DFT structural analysis of a series of atomically precise NCs, $Ag_{29-y}Au_y(BDT)_{12-x}(DHLA)_x$ (where y, x = 0,0; 0,1; 0,12 and 1,12; respectively) it was found that while the metal core is responsible for the origin of photoluminescence (PL), ligands play vital roles in determining their resultant PLQY.

INTRODUCTION

Noble metal nanoclusters (NCs) are composed of metal atoms and organic ligands (in general thiols) with distinct optical properties.[1-2] High photostability and ultrasmall sizes are the primary features of these metal NCs.[3-6] The significant disadvantage of these metal NCs in terms of their vis-nIR photoluminescence is their low quantum yield (PLQY) compared to semiconductor quantum dots (QDs).[7] Research strategies on improving the PLQY are in high demand, particularly for any PL-based application of metal NCs. Tuning the PLQY of metal NCs requires a fundamental understanding of their PL mechanism.[7] Questions such as the origin of PL, PL kinetics, the role of metal cores, ligands, etc. need careful consideration. Several reports exist on understanding the PL mechanisms of AuNCs. For example, Jin et al. reported that functional groups in the side chain of thiol ligands strongly influence the PL intensity of $Au_{25}(SR)_{18}$ NCs.[8] They inferred that thiol ligands with electron-rich atoms, such as O or N in the side chain, can promote the PL intensity through ligand to metal charge transfer (LMCT) or ligand to metal to metal charge transfer (LMMCT).[8] On the

other hand, a "kernel-origin" based PL mechanism was proposed by Aikens et al. through computational analysis.[9] It is conceivable that the kernel-structure relaxation is primarily responsible for the NIR emission of $Au_{25}(SR)_{18}$ NCs, rather than kernel-to-shell relaxation (i.e., Au(0) to Au(I)).[9] In another recent report, Jin et al. have supported such a "kernel-origin" mechanism by carefully choosing a correlated series of "monocuboctahedral kernel" AuNCs.[10] Results from such examples are summarized in a review article by Zhu et al.[7] The aggregation-induced emission (AIE) concept was proposed by the Xie group to explain the PL mechanism of AuNCs.[11-12] Considering these results, it is yet unclear whether the metal core (e.g., kernel-origin mechanism) or the 'ligand' (e.g., LMCT mechanism) is playing the dominant role in the PL properties of structurally known AuNCs. Furthermore, it has remained unclear whether these types of PL mechanism are general for all coinage-metal-based NCs or very specific to individual AuNCs only. In contrast to the latter, most of the coinage metal NCs with high QY are water-soluble,[13-14] and their structural details have not been elucidated to date.

$Ag_{29}(S_2R)_{12}$ NCs are one of the most studied fluorescent NCs from the silver family.[15-17] It is reported that by enhancing the structural rigidity[18] (which decreases the probability of nonradiative relaxation of the excited states) or by doping,[19] the PLQY of $Ag_{29}(BDT)_{12}$ NCs (BDT: 1,3-benzene-dithiol) can be significantly improved. For example, Zhu et al. reported that by lowering the temperature, ~20-fold enhancement in PLQY is achievable due to reduced nonradiative relaxation from excited states.[18] Bakr et al. showed 26-fold and 2.3-fold enhancement in the PLQY due to Au and Pt doping, respectively.[19] Zhu et al. have demonstrated 13-fold enhancement of the PLQY by adding excess triphenylphosphine (TPP), and aggregation-induced emission (AIE) was proposed as the prime reason for the enhancement. Pradeep et al. showed a nearly 30-fold enhancement of the PLQY by replacing such secondary TPP ligands with diphosphines of increasing chain length.[20] From DFT analysis, they proposed a LMCT mechanism to be responsible for the PLQY enhancement.[20] On the contrary, $Ag_{29}(DHLA)_{12}$ NCs (having the same chemical formula; DHLA: dihydrolipoic acid) do not have any such secondary ligands, but they are reported to have a higher PLQY than corresponding $Ag_{29}(BDT)_{12}$ NCs.[15, 21] The change of the PLQY could be due to structural differences or due to the effect of ligands. Notably, the presence of carboxyl groups in the thiol side chain (e.g., DHLA,[15, 22] mercaptosuccinic acid (MSA),[23] 11-mercaptoundecanoic acid (MUA),[14, 24] glutathione (GSH),[12, 25-26] etc.) is common in most of the water-soluble metal NCs with highest PLQY. The question arises if the carboxyl group promotes the PL, making LMMCT/LMCT the most dominant PL mechanism for the case of $Ag_{29}(DHLA)_{12}$ NCs? Since the crystal structure of $Ag_{29}(DHLA)_{12}$ NCs has not been solved yet, a different approach was taken here to characterize the structure of $Ag_{29}(DHLA)_{12}$ NCs, which can help to solve the puzzle of their PL mechanism.

In this work, we have employed a ligand exchange strategy starting with the structurally known $Ag_{29}(BDT)_{12}$ NCs[16] to understand the effect of ligands on the structure and optical properties of $Ag_{29}(DHLA)_{12}$ NCs. High-resolution electrospray ionization (HRESI) and ion mobility (IM) mass spectrometry (MS) confirmed the ligand exchange, leading to the formation of $Ag_{29}(BDT)_{12-x}(DHLA)_x$ NCs (x=1-6). This ligand exchange showed significant enhancement (~44 fold) in PLQY. Consequently, density functional theory (DFT) has been implemented to determine the most stable structure of single ligand exchanged $Ag_{29}(BDT)_{11}(DHLA)^{3-}$ (i.e. trianion species where only one BDT ligand had been exchanged by one DHLA ligand), which was further verified using ion size analysis by collisional cross-sections (CCS) determined via IM-MS experiments. This inference of the most stable isomer in $Ag_{29}(BDT)_{11}(DHLA)$ NCs led us to a likely structure of $Ag_{29}(DHLA)_{12}$ NCs, which has an icosahedral core with an $Ag_{16}S_{24}$ shell. Structural analysis of a series of atomically precise NCs, $Ag_{29-y}Au_y(BDT)_{12-x}(DHLA)_x$ (where y, x = 0,0; 0,1; 0,12 and 1,12; respectively) and experimental observations suggest that both ligand and core contribute to the PL properties of $Ag_{29}(DHLA)_{12}$ NCs.

RESULTS AND DISCUSSION

$Ag_{29}(BDT)_{12}$ and $Ag_{29}(DHLA)_{12}$ NCs were synthesized using reported protocols[15-16, 27] (see the methods section for details) and characterized using UV-vis absorption spectroscopy, fluorescence spectroscopy, and HRESI MS (Figure S1, S2, and S5). The ligand exchange experiment was performed by introducing an aqueous solution of DHLA to the purified $Ag_{29}(BDT)_{12}$ NCs in DMF (details are mentioned in the methods section, control experiments are in SI, Figure S16-S24). Note that, all the MS measurements in the current study were performed in negative ion mode. HRESI MS analysis of the resulting mixture shows the presence of NCs with a maximum of six ligands exchanged, which are assigned as $Ag_{29}(BDT)_{12-x}(DHLA)_x$ where x = 0-6, respectively based on their mass to charge ratio (m/z) and calculated isotopic pattern (Figure 1A, S3A, and S4). The magic behavior of NC with x=6 might be associated with their balanced structure due to the same ligand ratio. IM-MS has been employed to separate these six-ligand exchanged NCs based on their drift times in nitrogen (6.3, 6.9, 7.4, 7.7, 8.0, 8.3, and 8.6 ms for x = 0-6 ligand exchange products, respectively) (Figure 1B). Similar increase was observed in their respective collision cross sections (CCS) as well (480, 510, 533, 544, 558, 571 and 583 $Å^2$ for x = 0-6, respectively). The extent of ligand exchange was found to be nearly 20%, which was determined from the mass spectra peak intensity of the parent and ligand exchanged NCs. For this we have studied the relative intensities of the 3- charge state which we assume to be proportional to the solution concentration of the ensemble of NCs namely, $Ag_{29}(BDT)_{12-x}(DHLA)_x$ NCs (x = 1-6). It is important to note here that ligand exchange is mostly a dynamic process,[28] and hence it is expected that there will always be some unreacted or reverse ligand exchanged $Ag_{29}(BDT)_{12}$ NCs in the solution mixture. [28-30]

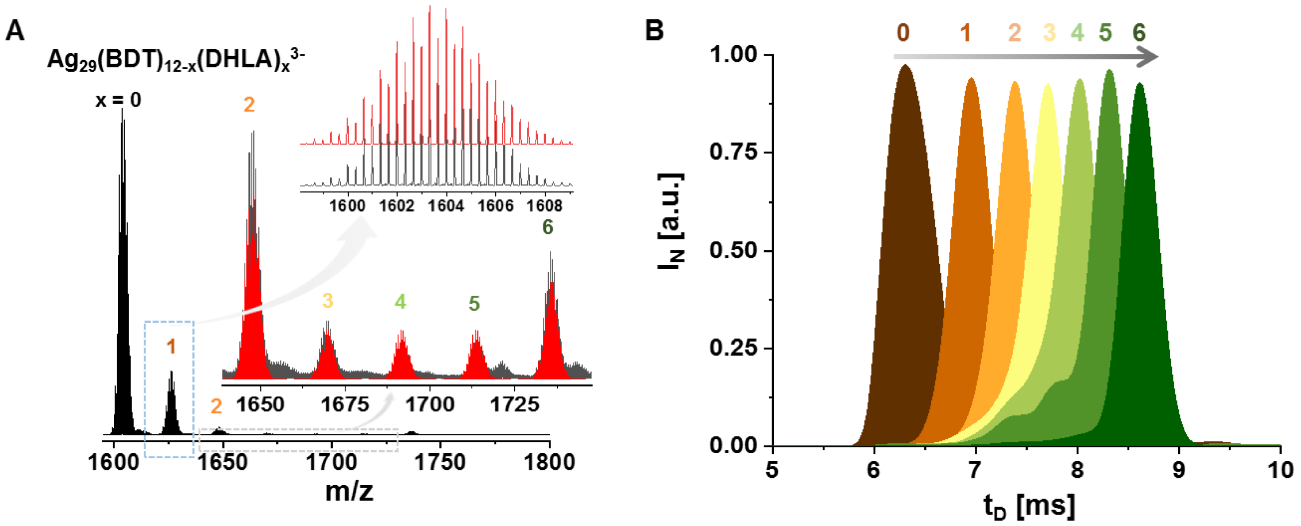

Figure 1. (A) Typical ESI MS of a $Ag_{29}(BDT)_{12-x}(DHLA)_x$ NCs solution showing a maximum of six ligands exchanged. An expanded view (black trace), is presented in the inset with corresponding calculated spectra (red trace). A further expanded view of the MS spectrum of $Ag_{29}(BDT)_{12-x}(DHLA)_x^{3-}$ with x=1 resolves the isotopologue distribution and shows an exact match with the calculated spectrum. (B) Drift time profile of $Ag_{29}(BDT)_{12-x}(DHLA)_x^{3-}$ measured in IM mode, showing the increasing size of the ligand exchanged NCs.

To understand how ligand exchange affects their optical properties, UV-vis absorption spectra were collected for $Ag_{29}(BDT)_{12-x}(DHLA)_x$ NCs and compared with $Ag_{29}(BDT)_{12}$ (Figure 2A) and $Ag_{29}(DHLA)_{12}$ NCs (Figure S5). The UV-vis absorption spectrum shows a nearly 11±3 nm blue-shift in the prime absorption peak (appears at 430±2 nm) in comparison to the parent $Ag_{29}(BDT)_{12}$ NCs, which has a peak situated at 441±3 nm (Figure 2A). Additionally, a new shoulder peak appears at 497 nm. Both of these two peaks show similarity with the absorption features (around 427±2 and 490±2 nm, respectively) of $Ag_{29}(DHLA)_{12}$ NCs (Figure S5). The shift in the absorption peak maximum due to ligand exchange suggests a significant role of the ligands on the optical band origins of the NCs. The emission spectrum of $Ag_{29}(BDT)_{12-x}(DHLA)_x$ NCs were collected to check the impact of ligand exchange on the PL intensities (Figure 2B). They are also presented in terms of a 2D PL map (Figure 2C). The spectra show 40±4-fold enhancement in PL intensity (Figure 2B) and no apparent shift in the maximum emission peak position (660 nm) (Figure 2B, C, S1B and S5). Maximum PL enhancement was seen at a DHLA concentration of 16.2 mM (Figure S8-S9), which was used for all further experiments. Bright photoluminescence can also be seen under a UV lamp in the case of $Ag_{29}(BDT)_{12-x}(DHLA)_x$ NCs (Figure 1A). The PLQY shows ~44-fold enhancement (PLQY of $Ag_{29}(BDT)_{12-x}(DHLA)_x$ NCs is 34.8%) upon ligand exchange on $Ag_{29}(BDT)_{12}$ NCs (PLQY =0.8%) (Figure S11, S12, and Table S1). This PLQY enhancement might be a contribution from one single NC or combination of all NCs. The ligand exchange kinetics was monitored based on the change in intensity of the emission peak (at 660 nm) and the change in absorption peak position (from 441 nm of the parent $Ag_{29}(BDT)_{12}$ NCs). The PL intensity plot has a sigmoidal shape (Figure 2D and S10), and it takes nearly 200±10 minutes to complete the ligand exchange process. Reverse ligand-exchange on $Ag_{29}(DHLA)_{12}$ NCs using BDT (Figure S16-17) shows a decrease in PL intensities, further supporting the decisive role of ligands on the PL.

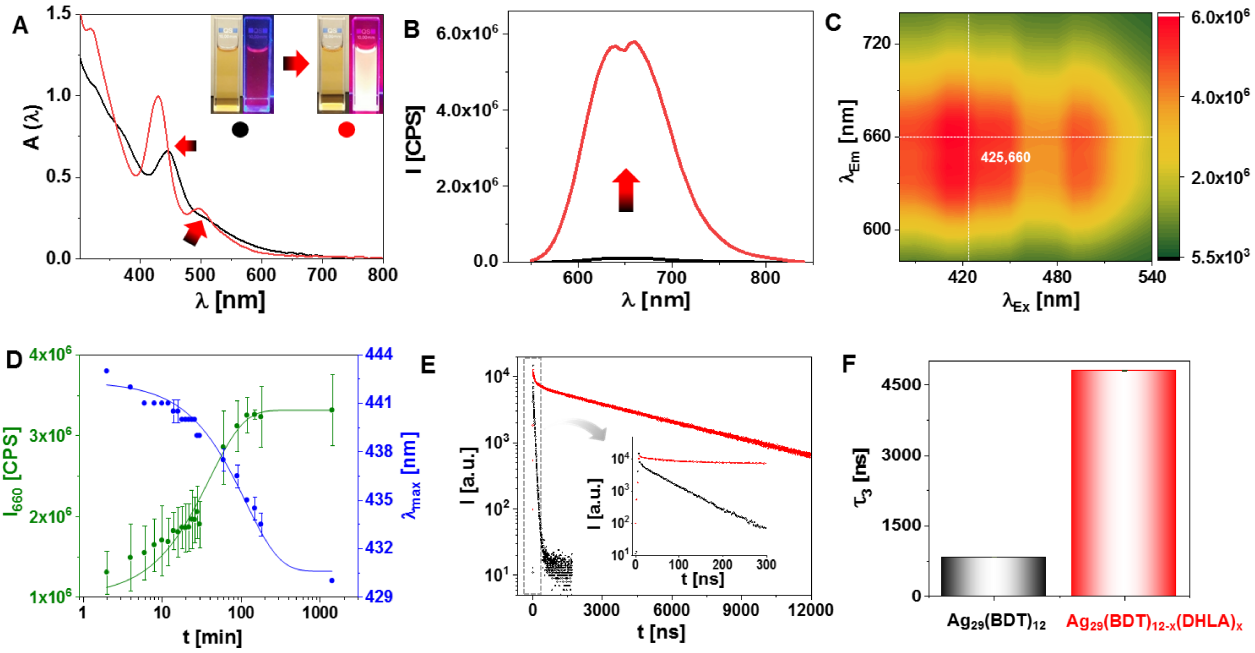

Figure 2. (A) UV-vis absorption spectra of $Ag_{29}(BDT)_{12}$ NCs (black trace) and $Ag_{29}(BDT)_{12-x}(DHLA)_x$ NCs (red trace). The inset shows the corresponding photographs of $Ag_{29}(BDT)_{12}$ NCs (black dot) in DMF and $Ag_{29}(BDT)_{12-x}(DHLA)_x$ NCs (red dot) in a DMF-water mixture under visible (left) and UV (right) light, respectively. (B) PL spectra of $Ag_{29}(BDT)_{12}$ NCs (black trace) and $Ag_{29}(BDT)_{12-x}(DHLA)_x$ NCs. The PL intensity at 660 nm were used for relative comparison. (C) 2D PL map of $Ag_{29}(BDT)_{12-x}(DHLA)_x$ NCs. (D) Kinetics of ligand exchange monitored by the PL intensity at 660 nm (green dots) and the wavelength corresponding to the maximum absorbance (blue dots) of $Ag_{29}(BDT)_{12-x}(DHLA)_x$ NCs. (E) Lifetime decay curves of $Ag_{29}(BDT)_{12}$ NCs (black trace) and $Ag_{29}(BDT)_{12-x}(DHLA)_{12}$ NCs (red trace). The inset shows the expanded view of the decay curves. (F) Column plot of the corresponding longer lifetime component values (τ_3) derived from the lifetime data (details in SI).

The ligands' contribution to enhancing the PLQY could be due to these three reasons: a) AIE, b) surface rigidification, or c) LMCT, as explained previously in a few specific cases.[7] Initially, a decrease in the pH of the solution does not result in enhanced PL intensity in the ligand exchanged NCs (Figure S19), so AIE can be ruled out.[31-32] Surface rigidification (apart from AIE) can happen due to other intra-ligand interactions in the NCs. This cannot be completely ruled out because the NCs' carboxyl group and benzene ring might have intra-ligand interaction.[33] The other possibility is that the carboxyl group can form dimers, which has been observed in the case of many carboxylic acids.[34-36] Such bonding interaction between the ligands (of the same NC) reduces molecular flexibility in the solution, reducing the nonradiative relaxation, thus resulting in enhanced PLQY. Another possibility is to enhance the PLQY via LMCT, which we attribute to be the dominating mechanism in our work, as the carboxyl functional group is known for promoting LMCT due to electron-donating atoms (oxygen).[37]

To unravel the mechanism further, time-resolved spectroscopy data of $Ag_{29}(BDT)_{12}$ and $Ag_{29}(BDT)_{12-x}(DHLA)_x$ NCs were compared (Figure 2E, Figure S15 and Table S2). We found a substantial increase in the PL lifetime when substituting BDT with DHLA. The lifetime data were fitted using a tri-exponential decay (Figure S15), resulting in two shorter (τ_1 and τ_2) and one longer (τ_3) lifetime components (Table S2). In general, for thiolated metal NCs, the shorter lifetime components (τ_1 and τ_2) are usually attributed to the interband transition (d → sp) of the metal cores. In contrast, the longer lifetime component (τ_3) might correspond to the LMCT transition.[7, 43-45] In the case of the ligand-exchanged $Ag_{29}(BDT)_{12-x}(DHLA)_x$ NCs, τ_3 increased to 4.79 μs and became the dominating (98%) contributor (Figure 2F, Table S2). This result suggests an important contribution of ligands in the PL mechanism and raises the question about the ligands' orientation on the NCs' surface, which needs a structural understanding of the ligand-exchanged NCs.

To obtain the molecular structure (see the methods section for details), the coordinates of $Ag_{29}(BDT)_{12}$ were taken from Abdul et al.[16] There are 12 BDT ligands that consist of six symmetry equivalent pairs in the NC, giving two possible thiol sites for the addition of DHLA. As each BDT ligand has two thiol groups, this allows one doubly deprotonated (protons from -SH group) DHLA ligand to replace a single BDT group. The TPP ligands also present in the solid were removed as they are not present in the $Ag_{29}(DHLA)_{12}$ NCs. Four possible isomers were created for $Ag_{29}(BDT)_{12-x}(DHLA)_x^{3-}$(x=1) using the MacMolPlt visualization tool, and the connectivity to the thiol groups can be seen in Figure 3.[46] The thiol groups guide the construction of the ligand, so the distance between thiol sites was measured,

as well as the distance between the same thiol site on the neighboring ligand (6 ligand pairs or 'neighbors' making 12 total ligands in the cluster).

The average bond lengths calculated at the BP86/DZ level of the theory of the ground state structure upon the addition of ligands are shown in table 1.

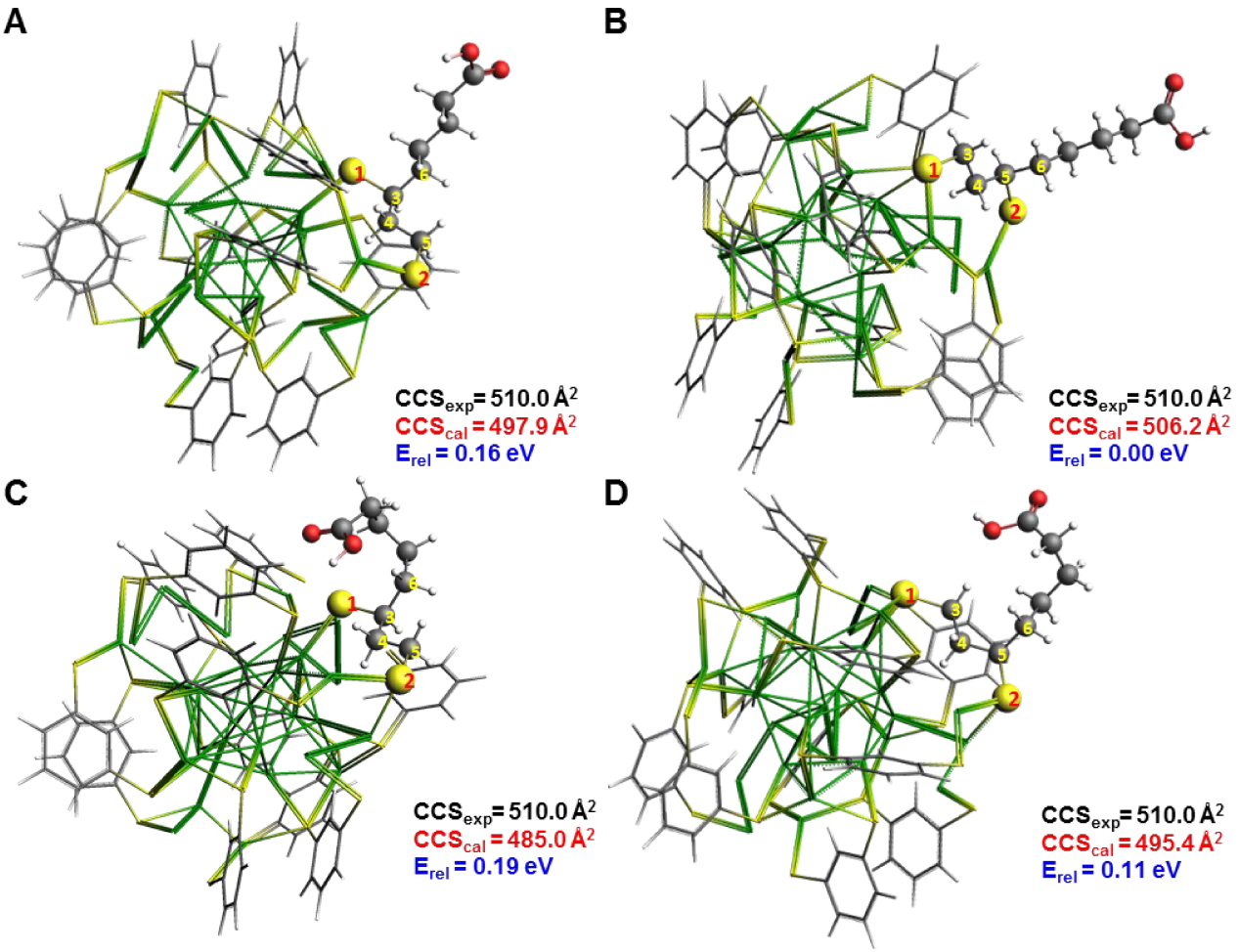

Figure 3. Molecular structures of the four isomers created for $Ag_{29}(BDT)_{11}DHLA^{3-}$. The green, yellow, grey, red, and white atoms represent silver, sulfur, carbon, oxygen, and hydrogen. All four isomers kept the thiol group locations from the crystal structure in place (atoms 1 and 2). (A) The trans A structure sticks out with 180 dihedral angles ~14.20 Å away from the center of the icosahedral core. The DHLA ligand was constructed by starting at thiol group 2 and connecting atoms 2-5-4-3-6 with thiol group 1 connecting to carbon atom 3. (B) The trans B structure also sticks out with 180 dihedrals, with the same distance away from the core. The DHLA ligand was constructed by starting at thiol group 1 and connecting atoms 1-3-4-5-6 with thiol group 2 connecting to carbon atom 5. (C) The curled A structure has the same connectivity as Trans A; however, it is curled around the NC to observe the interaction between the carboxyl group and outer shell Ag motif. (D) The curled B structure has the same connectivity as Trans B, and it is also curled around the NC like the Curled A structure. The calculated most stable isomer (Trans B) is in agreement with the corresponding experimental data, as revealed by a close match between CCS values (exp and cal). All the CCS were calculated using trajectory method as implemented in IMOS 1.09 taking the different isomeric DFT optimized structures and assuming the 3- charge was distributed following Natural Population Analysis (NPA).We have also included the quadrupole moment of N_2 in the CCS calculation.[47]

As the DHLA ligands are added, the Ag_{13} icosahedral core and the Ag-Ag shell bonds elongate. Elongation in the core specifically happens in the outer part of the icosahedron, where bonds not involving the center atom can get up to ~0.040 Å longer and others ~0.035 Å shorter as seen in Figure S25. Elongation in the core and shell is generally consistent as each DHLA ligand is added. Eventually, the average difference between $Ag_{29}(BDT)_{12}$ and $Ag_{29}(DHLA)_{12}$ is 0.003 Å in the core and 0.054 Å in the shell. The Ag-S bonds (both crown and motif positions,

Figure 4C in the main paper) shorten by ~0.005 Å between $Ag_{29}(BDT)_{12}$ and $Ag_{29}(DHLA)_{12}$ NCs. The distance between thiol sites ('1' and '2', Figure 3) gets slightly larger with the addition of DHLA. The thiol sites between neighboring ligands (site '1' compared with site '1' on the closest neighboring ligand) do not show a common trend; however, this distance does increase when all 12 DHLA ligands are added as compared to 12 BDT ligands. Therefore, the surface configuration does change in conjunction with the thiol groups.

[Å]	Ag core-Ag core	Ag shell-Ag shell	Ag shell-S crown	Ag shell-S motif	S thiol-S thiol	S group-S group
$Ag_{29}(BDT)_{12}$	2.962 ± 0.310	2.984 ± 0.021	2.564 ± 0.015	2.619 ± 0.040	5.680 ± 0.015	4.389 ± 0.043
$Ag_{29}(BDT)_{11}DHLA$	2.962 ± 0.307	2.992 ± 0.025	2.563 ± 0.016	2.621 ± 0.044	5.684 ± 0.023	4.391 ± 0.038
$Ag_{29}(BDT)_{10}(DHLA)_2$	2.963 ± 0.308	2.994 ± 0.027	2.563 ± 0.017	2.621 ± 0.051	5.689 ± 0.030	4.388 ± 0.051
$Ag_{29}(BDT)_9(DHLA)_3$	2.963 ± 0.307	2.990 ± 0.032	2.563 ± 0.019	2.619 ± 0.049	5.697 ± 0.034	4.374 ± 0.048
$Ag_{29}(BDT)_8(DHLA)_4$	2.964 ± 0.306	2.994 ± 0.029	2.563 ± 0.020	2.618 ± 0.049	5.699 ± 0.030	4.388 ± 0.058
$Ag_{29}(DHLA)_{12}$	2.965 ± 0.306	3.038 ± 0.038	2.56 ± 0.021	2.615 ± 0.043	5.736 ± 0.017	4.480 ± 0.032

Table 1. Average bond lengths of the optimized structures upon the addition of DHLA in Å.

The ground state (S_0) geometry optimization was run for each trianion isomer with x=0-4 and 12. The most stable energy isomer is Trans B, which can be seen in Figure 4A (labelled **a**).

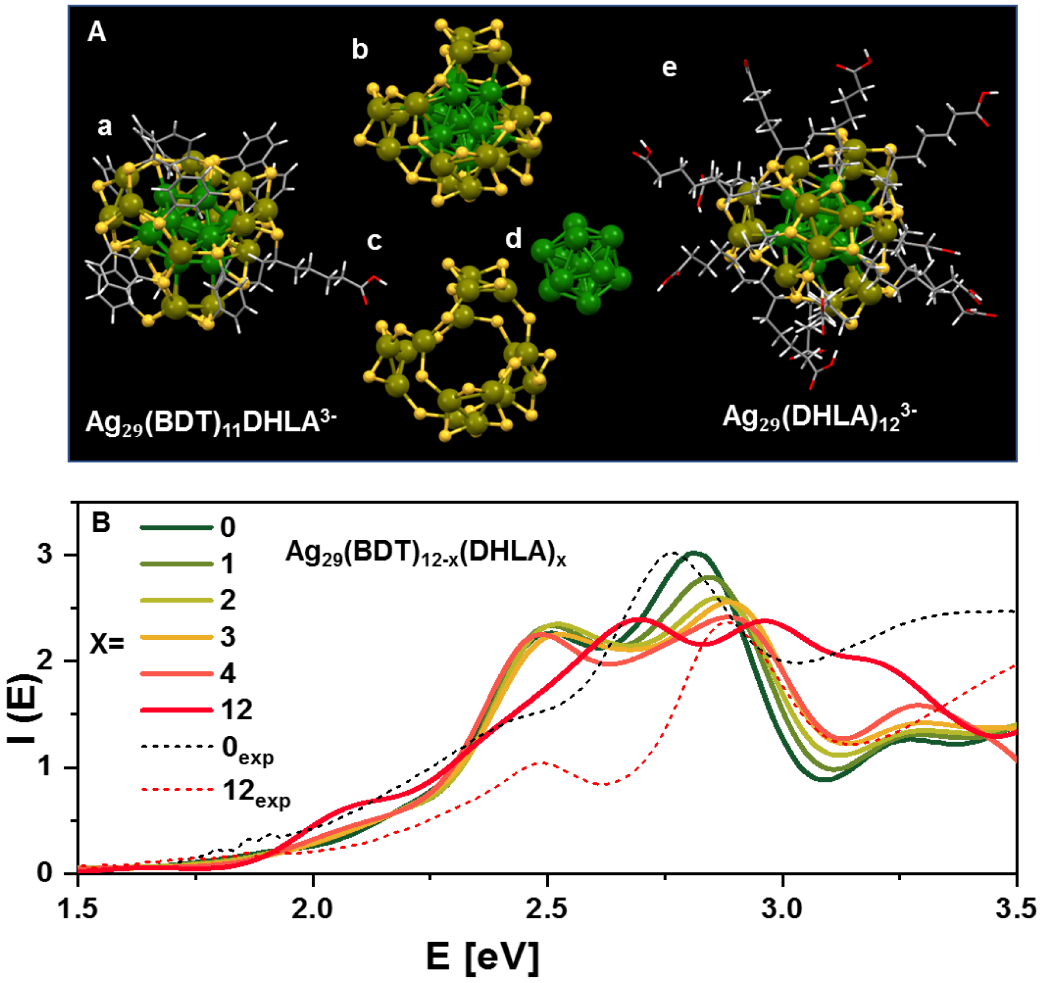

Figure 4. (A) Molecular structures of the lowest energy isomers of $Ag_{29}(BDT)_{11}DHLA^{3-}$ (a) and $Ag_{29}(DHLA)_{12}^{3-}$(e). The green atoms (deep green are in the core and olive green are in the shell) are silver, yellow atoms are sulfur, grey are carbon, white are hydrogen, and red are oxygen. (a) The entire 187-atom NC with one BDT ligand replaced by one DHLA ligand. (b) The structure without the organic part containing an icosahedral core with an $Ag_{16}S_{24}$ shell. (c) $Ag_{16}S_{24}$ shell made of four Ag_3S_6 crowns with four Ag_1S_3 motifs. (d) The 13-atom icosahedral core. (e) The entire 341-atom $Ag_{29}(DHLA)_{12}$ NC. Each BDT group has now been replaced by the corresponding DHLA group. (B) Absorption spectra calculated for $Ag_{29}(BDT)_{12-x}(DHLA)_x^{3-}$(x=0-4,12) together with the experimental spectra of $Ag_{29}(BDT)_{12}$ (black dotted line) and $Ag_{29}(DHLA)_{12}$ NCs (red dotted line), respectively. I (E) is proportional to [Absorbance/(Energy)^2].

For further confirmation, CCS values have been measured using IM-MS[47] and were compared with the corresponding calculated values (Figure 3) (details of the CCS calculations are mentioned in SI). The close match of the experimental CCS values with the calculated ones for Trans B isomer strengthens the theory-experimental correlation. While the theory and experiment agree that the lowest energy isomer is the Trans B structure, and hence we use it for further computational study, we cannot exclude the possibility that other isomers may exist in solution. The relative energies vary between isomers from 0.03 eV – 0.5 eV depending upon the level of theory and are reported in the supporting information. However, to understand exactly how the alkane chain in DHLA transforms in solution, dynamics calculations would be required.

Predicted absorption spectra for $Ag_{29}(BDT)_{12-x}(DHLA)_x$ NCs are in good agreement with the experimental results (Figure 4B). When x=0, the higher energy peak appears at 2.80 eV, which corresponds to the experimentally observed peak at 2.76 eV. The lower energy peak appears at 2.52 eV, which corresponds to the experimentally observed shoulder at 2.43 eV. Upon the addition of DHLA, both peaks blue shift. The higher energy peak appears at 3.02 eV, and the lower energy peak appears at 2.68 eV. This blue shift of both peaks upon the addition of DHLA also appears in the experimental spectrum (Figure S5, S10, and Figure 2D). The PL of $Ag_{29}(BDT)_{12-x}(DHLA)_x$ NCs are analyzed by running an excited singlet state geometry optimization from the optimized ground state (S_0) geometry (for trianions). The emission energy is calculated by taking the difference between the excited and ground-state energies at the optimized excited state geometry (details are in the SI). Triplet states could not be accessed as there were SCF convergences issues at the BP86/DZ level of theory. The theoretical emission energy, 0.84 eV, is significantly underestimated compared to the experimental PL spectrum centered at 1.91 eV. The geometry and HL gaps of our optimized S_1 state are shown in the supporting information; however, due to the neglect of spin orbit coupling and only analyzing stationary points on adiabatic states, there are limitations to understanding the PL mechanism from a theoretical perspective. Consequently, the calculations with long-range exchange-correlation functional, presented in the supporting information, hint that the PL mechanism may primarily arise from metal to metal transitions.

To reveal the metal kernel's role on the optical properties, the $Ag_{29}(DHLA)_{12}$ NCs were doped with Au via a post-synthesis modification route with different doping percentage (synthesis details and characterizations are mentioned in the SI, Figure S6 and S7). A 4-fold increase in the PLQY of $Au_yAg_{29-y}(DHLA)_{12}$ was observed in comparison to $Ag_{29}(DHLA)_{12}$ NCs (Figure S13-14 and Table S1). The average lifetime decreased from 3.7 μs (in $Ag_{29}(DHLA)_{12}$ NCs) to 1.5 μs (in $Au_yAg_{29-y}(DHLA)_{12}$ NCs) upon doping (Figure S15 and Table S2). So, the results suggest that even single Au atom doping (Figure S28 and S30C) can result in an enhancement in PLQY of $Ag_{29}(DHLA)_{12}$ NCs, and hence the contribution of the metal core in the PL mechanism cannot be ignored. DFT structural analysis (of trianions) suggests that a single Au atom doping in $Ag_{29}(DHLA)_{12}$ NCs can change the HOMO-LUMO gap significantly from 1.24 to 1.37 eV (a similar trend has been observed upon doping $Ag_{29}(BDT)_{12}$ NCs); on the other hand, a single ligand exchange does not affect the HOMO-LUMO gap (Figure 5A). $Ag_{29}(BDT)_{12-x}(DHLA)_x$ NCs have structural similarities, but the increase in experimental PLQY shares specific patterns with the theoretical ground state analysis. Both gold mono-doping and exchanging the ligands to DHLA increase the Ag-Ag shell bond lengths while simultaneously shortening the Ag-S bonds. The average core bond lengths change less than ~0.006 Å, which hints that the core's average structural differences may not be the only contribution to the enhanced experimental PLQY. Still, a consistent blue shift in both experimental absorption and emission peaks upon doping suggests the core structure is responsible for the origin of PL in $Ag_{29}(DHLA)_{12}$ NCs.

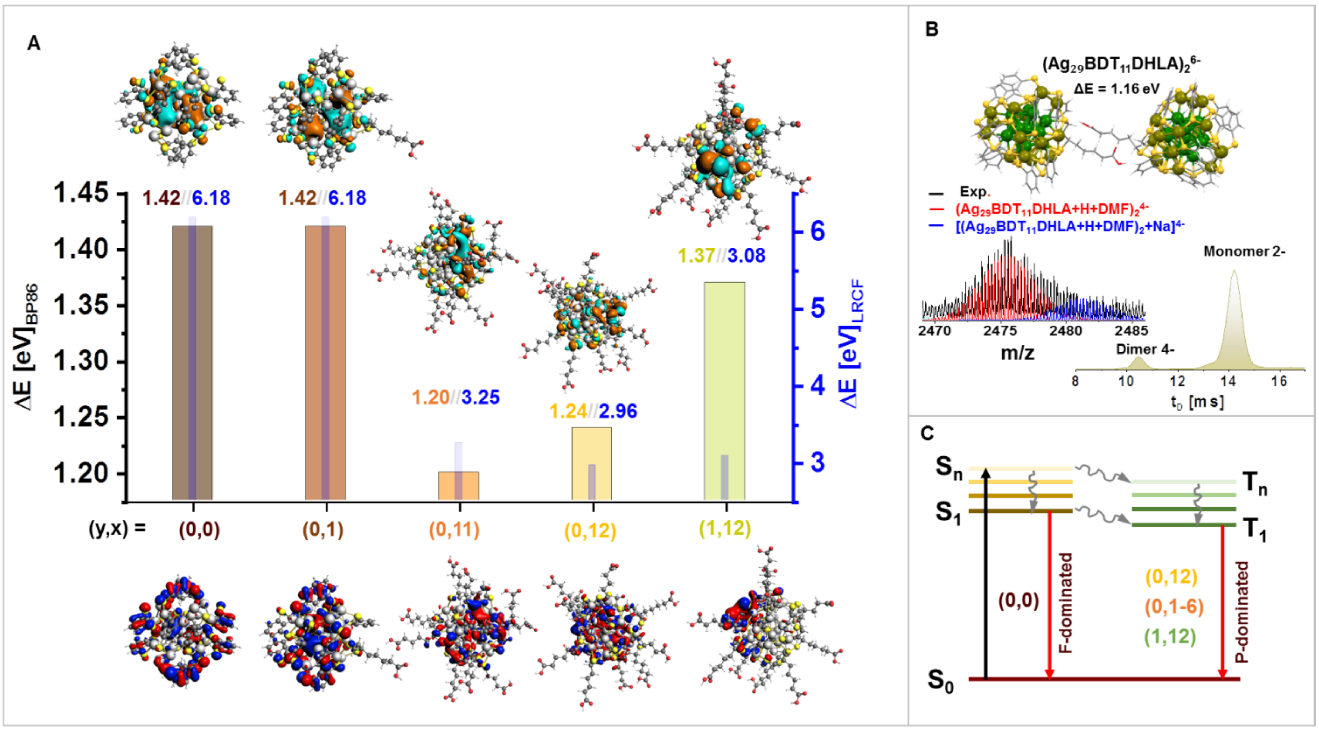

Figure 5. (A) The HOMO-LUMO energy gaps of a series of $Ag_{29-y}Au_y(BDT)_{12-x}(DHLA)_x^{3-}$(where y, x = 0,0; 0,1; 0,11; 0,12 and 1,12; respectively). Blue column (right axis) represents the energy gap via LRCF calculation, whereas the other color column represents the energy gap via BP86 calculation, together with their corresponding representative HOMO (down side) and LUMO structures (upper side), respectively. (B) DFT optimized dimer structure of $(Ag_{29}(BDT)_{11}DHLA)_2^{6-}$ with a calculated HOMO-LUMO gap of 1.16 eV. Dimers were identified from IM-MS as shown in B. Extracted MS from the 10-11 ms region in the mobilogram (labeled as

dimer 4-) is shown in the inset, which shows an exact match with the isotopologue distribution expected for the 4- dimer of $Ag_{29}(BDT)_{11}DHLA$ NC with a few solvent molecules. (C) Jablonski diagram illustrating the proposed dominating relaxation mechanism for each $Ag_{29-y}Au_y(BDT)_{12-x}(DHLA)_x^{3-}$ NC cases (marked as (y, x)). The energy levels are drawn in a qualitative way and does not reflect their accurate energies.

While the excitations within the core might be the origin of the PL, ligands play a vital role in the PLQY especially for the case of $Ag_{29}(BDT)_{12-x}DHLA_x$ NCs. Experimentally, the PLQY can be enhanced in two ways, either by increasing the radiative contribution or by decreasing the nonradiative contribution (i.e., surface vibration and ultrafast structural relaxation).[7] In this case, the ligand exchange leads to a considerable decrease in nonradiative relaxation (~100-fold decrease in the qualitative K_{NR} value as revealed from their lifetime data, Table S3). A decreasing contribution of nonradiative relaxation in $Ag_{29}(BDT)_{12-x}DHLA_x$ NCs could be due to additional intra-NC ligand interaction (between BDT and DHLA) or due to intra-NC interaction via dimer formation (please note that polymer formation or the possibility of aggregation has already been excluded – see above). Using IM-MS, we could confirm dimer formation in the solution and obtained corresponding MS data representing dimers of $Ag_{29}(BDT)_{11}DHLA$ NCs (Figure 5B). The existence of proton and Na ion bound dimers has been reported for $Ag_{29}(BDT)_{12}$ NCs.[48] The DFT optimized structure of the dimer multianions revealed a smaller HOMO-LUMO gap (1.16 eV) than the parent NC (1.42 eV). The concentration-depended shift in their PL emission maxima (Figure S5) further confirms dimers' existence in the solution. The formation of dimers leads to a decrease in molecular flexibility, minimizing the nonradiative relaxation and, hence, the increase in PLQY. However, that alone might not explain 44-fold PLQY enhancement in the ligand-exchanged NCs. Understanding the PL mechanism would be needed to explain this high PLQY. The lifetime dynamics for $Ag_{29}(BDT)_{12}$ NCs show the highest contribution (93%) from τ_2, whereas for ligand exchanged NC, $Ag_{29}(DHLA)_{12}$ and Au-doped NC cases, it comes from τ_3. The longer lifetime (in the range of μs) indicates triplet states' involvement via intersystem crossing, which supports the major contribution of phosphorescence (which involves LMCT) in their PL mechanism. In contrast, fluorescence is dominating for the case of $Ag_{29}(BDT)_{12}$ NC (Figure 5c). Solvent induced shift confirms the charge transfer[38-42] in the excited states (Figure S21) and O_2-induced PL quenching confirms (Figure S24) the involvement of triplet states and provides a strong proof of LMCT.[15] The differences in ligands backbone structure play an important role in facilitating the charge transfer process in the following two ways.

Firstly, the electron-donating capacity of the DHLA ligand is more than the BDT ligand (due to delocalization and involvement in additional π - π inter-ligand interactions), which facilitates the charge transfer via Ag-S bonds to the metal core. The addition of ligands with multiple electrons donating groups results in enhancing the PL intensity, supporting the above statement (Figure S20). Secondly, the free carboxyl group can be further involved in intra-NC (when one of the thiols ends is not attached to Ag) and inter NC (for dimers) charge transfer via carboxyl group as seen for glutathione protected Au_{25} NCs.[8] This is supported by the pH-dependent experiment where deprotonation enhances the PL intensity (Figure S19).

CONCLUSIONS

In summary, we have shown how ligand exchange can tune the structure, and optical properties of $Ag_{29}(S_2R)_{12}$ NCs. Ligand exchange with DHLA ligands on $Ag_{29}(BDT)_{12}$ NCs showed ~ 40-fold enhancement in PLQY. Extensive DFT calculation predicts the structure, optical, and photo-physical properties of $Ag_{29}(BDT)_{12-x}DHLA_x^{3-}$ (x=1, 12). CCS comparison based on IM-MS and trajectory calculations confirms a good match of the DFT-predicted structure with the experimental one. The photoluminescence mechanism involves both the fluorescence and phosphorescence processes. However, based on the lifetime dynamics analysis, fluorescence is major contributor in Ag_{29} NCs with x=0, whereas phosphorescence dominates in x=1-12 and even for Au doped NCs. The involvement of the triplet state suggests that the PLQY enhancement is due to LMCT. Ligand's structure and orientation play a major role in the LMCT process. DHLA being more electron-donating than BDT, facilitates the charge transfer via Ag-S bond to metal core.

Furthermore, the carboxyl group of the DHLA can also promote inter-NC and intra-NC charge transfer. Additionally, nonradiative relaxation is relatively less significant in $Ag_{29}(BDT)_{12-x}DHLA_x^{3-}$ (x=1-6) due to the dimer formation, enhancing the structural rigidity and thus the resulting enhancement in the PLQY. Hence, although the core might be responsible for photoluminescence's origin, the ligand plays a vital role in determining their PLQY. Surface engineering on ligands or doping in the core can affect the PL intensity and the PLQY, but tunability in emission wavelength is achievable via doping for $Ag_{29}(DHLA)_{12}$ NCs. This result also suggests that the PL mechanism is specific to individual NCs, where 'every metal atom and ligand matters', unlike semiconductor QDs. The ligand's structure and functionality in NCs could be a potential key in solving the mystery of the PL of metal NCs.

EXPERIMENTAL SECTION

Synthesis of $Ag_{29}(BDT)_{12}$ NCs. $Ag_{29}(BDT)_{12}$ NCs were synthesized using a previously reported protocol[16] with slight modifications. More specifically, 10 mL of dicholormethane (DCM) was mixed with 13.5 µL of BDT in a 20 mL borosilicate glass scintillation vial. Then, a solution of 20 mg $AgNO_3$ in 5 mL methanol was added to the reaction mixture under vigorous stirring, whereby the color of the reaction mixture turned turbid yellow due to the formation of insoluble Ag-S complex. A solution of 200 mg TPP in 2 mL of DCM was then added and allowed to stir for 10 minutes, during which the solution turned colorless due to the formation of Ag-S-P complex, which completely dissolves under such reaction conditions. Shortly after that, 500 µL of 0.555 M freshly prepared $NaBH_4$ solution was

added under vigorous stirring and the solution turned dark brown immediately. After 10-12 h the solution turned orange, indicating the formation of $Ag_{29}(BDT)_{12}$ NCs. The as-prepared NCs were centrifuged at 9000 rpm for 2 minutes, the supernatant was discarded, and the pellet was washed several times with ethanol. The purified NCs were allowed to dry overnight under vacuum and were then re-suspended in DMF for further work.

Synthesis of $Ag_{29}(DHLA)_{12}$ NCs. $Ag_{29}(DHLA)_{12}$ NCs were synthesized according to a previously reported method[27] with some modifications. Briefly, 19 mg of (±)-α-lipoic acid (LA) and 7 mg $NaBH_4$ were added in 14 mL MilliQ water under vigorous stirring until LA was dissolved completely. 700 µL 25 mM $AgNO_3$ was added to the 14 mL solution and the solution color changed to muddy and pale yellow. Next, 10 mg NaBH4 dissolved in 2 mL water were added to the solution and the color changed to brown. The solution was stirred at 1500 rpm in the dark at room temperature for 4.5 h and the color changed to orange at the end. The NCs were stored at 4 °C in the dark for further work. For mass spectrometry analysis of $Ag_{29}(DHLA)_{12}$ NCs, $NaBH_4$, and NaOH were replaced by tetramethylammonium borohydride (TMAB) and ammonium hydroxide (NH_4OH).[15]

Ligand exchange of $Ag_{29}(BDT)_{12}$ NCs. The ligand exchange of $Ag_{29}(BDT)_{12}$ NCs was carried out using different concentrations of LA. In a typical experiment, different amounts of LA (0 mM, 8.1 mM, 16.2 mM, 32.3 mM, 48.5 mM, and 96.9 mM; all referring to final concentrations) and 15 mg $NaBH_4$ were dissolved in 2 mL of water and were mixed with 1 mL of $Ag_{29}(BDT)_{12}(TPP)_4$ NCs in DMF solution and allowed to react overnight. The reaction vials were kept in the dark at room temperature.

Synthesis of Au-doped $Ag_{29}(DHLA)_{12}$ NCs. The Au-doped $Ag_{29}(DHLA)_{12}$ NCs were synthesized following the literature with some modifications.[49] 500 µL MilliQ water was added to 1 mL freshly prepared $Ag_{29}(DHLA)_{12}$ NCs in glass bottles, and 30 µL of 1, 5, 10, 15, 20 and 25 mM $HAuCl_4$ were added into the NC solutions separately. The solutions were vigorously stirred in the dark and room temperature. After 30 minutes, 10 µL 1 mg/mL DHLA and 1 mg $NaBH_4$ were added into these seven solutions separately, and the solutions were stirred for 18 h.

Synthesis of Au-doped of $Ag_{29}(BDT)_{12}$ NCs. The Au-doped $Ag_{29}(BDT)_{12}$ NCs were synthesized following the method reported by Soldan *et al.*[19] with slight modification. In brief, $HAuCl_4$ stock solution (23.6 mM) was prepared in methanol and TPP stock solution (94.4 mM) was prepared in DCM. To 1.5 mL of $HAuCl_4$ stock solution, 2.5 mL of methanol was added and was mixed with 750 µL of TPP stock solution and 250 µL of DCM under vigorous stirring for 20 minutes. The color turned turbid white. Then, 14 mg of $AgNO_3$ was added and allowed to stir for 10 minutes. Shortly after that, 13.5 µL of BDT was added to the reaction mixture and stirred for 5 minutes, followed by the addition of 200 mg of TPP during which the solution turned colorless. *Then, 500* µL of 0.555 M freshly prepared $NaBH_4$ solution was added to the reaction mixture and the solution was continued to stir overnight protected from direct light. The as-prepared NCs were centrifuged at 9000 rpm for 2 minutes, the supernatant was discarded, and the pellet was washed several times with methanol. The purified NCs were allowed to dry overnight under vacuum and were then re-suspended in DMF for further work.

Computational details. All calculations were done using the Amsterdam Density Functional (ADF) 2017.110 and 2018.105 packages.[50] All geometry optimizations (ground and excited state) were calculated with the generalized gradient approximation (GGA) BP86 exchange-correlation functional[51-52] and a double zeta (DZ) basis set. All structures were optimized in the gas phase. Scalar relativistic effects were included by utilizing the zeroth-order regular approximation (ZORA).[53-54] Any dispersion calculations were completed by adding the Grimme1 dispersion correction to the exchange- correlation functional.[55-56] The energy and gradient convergence criteria were tightened to $1x10^{-4}$ and $1x10^{-3}$ respectively for geometric accuracy. After the initial ground state geometry optimization, a linear response time-dependent density-functional theory plus tight binding[57] (TDDFT+TB) calculation was run to obtain vertical (singlet) excitation energies which are then convolved into the optical absorption spectrum with a Gaussian fit with a 0.20 eV full width half maximum. This method is very similar to TDDFT; however, it allows us to reach higher energies of the absorption spectrum at a lower computational cost. After obtaining the ground state structure and absorption spectrum, TDDFT excited-state gradients[58] were used to optimize the structure of the first singlet excited state.

ASSOCIATED CONTENT

Supporting Information: This material is available via the Internet. Experimental details, ESI MS spectra, PL lifetime data, PL quantum yield calculations, lifetime data, pH-dependent data, kinetics data, several control experiments and computational details (Figure S25-34). This material is available free of charge via the Internet at http://pubs.acs.org.

AUTHOR INFORMATION

Corresponding Authors

*E-mail: wolfgang.parak@uni-hamburg.de
cmaikens@ksu.edu
indranath.chakraborty@physik.uni-hamburg.de

Notes

The authors declare no competing financial interest.

ACKNOWLEDGMENT

The authors acknowledge the financial support for this work offered by the Deutsche Forschungsgemeinschaft (DFG) project ID 390715994 and BA 3580/22-1 and PA 794/28-1. Y. Z. was supported by the Chinese Scholarship Council (CSC). I. C. thanks Fonds der Chemischen Industrie im Verband der Chemischen Industrie for support. S.H. and C.M.A. were supported by the National Science Foundation (CHE-1905048) of the United States. The computing for this work was performed on the Beocat Research Cluster at Kansas State University, which is funded in part by NSF grants CHE-1726332, CNS-1006860, EPS-1006860, and

EPS-0919443. S.H. further thanks Pratima Pandeya for the creation of the general bond analysis script in python. M.M.K. and A.B. thanks Karlsruhe Nano Micro Facility (KNMF) and KIT for use of the mass spectrometry facility. A.B. thanks Erik Karsten Schneider for CCS calculations.

REFERENCES

1. Chakraborty, I.; Pradeep, T., Atomically Precise Clusters of Noble Metals: Emerging Link between Atoms and Nanoparticles. *Chem. Rev.* **2017,** *117* (12), 8208-8271.
2. Jin, R.; Zeng, C.; Zhou, M.; Chen, Y., Atomically Precise Colloidal Metal Nanoclusters and Nanoparticles: Fundamentals and Opportunities. *Chem. Rev.* **2016,** *116* (18), 10346-10413.
3. Zheng, K.; Yuan, X.; Goswami, N.; Zhang, Q.; Xie, J., Recent advances in the synthesis, characterization, and biomedical applications of ultrasmall thiolated silver nanoclusters. *RSC Adv.* **2014,** *4* (105), 60581-60596.
4. Genji Srinivasulu, Y.; Yao, Q.; Goswami, N.; Xie, J., Interfacial engineering of gold nanoclusters for biomedical applications. *Mater. Horiz.* **2020,** *7* (10), 2596-2618.
5. Mathew, A.; Pradeep, T., Noble Metal Clusters: Applications in Energy, Environment, and Biology. *Part. Part. Syst. Charact.* **2014,** *31* (10), 1017-1053.
6. Shang, L.; Dong, S.; Nienhaus, G. U., Ultra-small fluorescent metal nanoclusters: Synthesis and biological applications. *Nano Today* **2011,** *6* (4), 401-418.
7. Kang, X.; Zhu, M., Tailoring the photoluminescence of atomically precise nanoclusters. *Chem. Soc. Rev.* **2019,** *48* (8), 2422-2457.
8. Wu, Z.; Jin, R., On the ligand's role in the fluorescence of gold nanoclusters. *Nano Lett.* **2010,** *10* (7), 2568-2573.
9. Weerawardene, K. L. D. M.; Aikens, C. M., Theoretical Insights into the Origin of Photoluminescence of $Au_{25}(SR)_{18}^-$ Nanoparticles. *J. Am. Chem. Soc.* **2016,** *138* (35), 11202-11210.
10. Li, Q.; Zhou, M.; So, W. Y.; Huang, J.; Li, M.; Kauffman, D. R.; Cotlet, M.; Higaki, T.; Peteanu, L. A.; Shao, Z.; Jin, R., A Mono-cuboctahedral Series of Gold Nanoclusters: Photoluminescence Origin, Large Enhancement, Wide Tunability, and Structure–Property Correlation. *J. Am. Chem. Soc.* **2019,** *141* (13), 5314-5325.
11. Luo, Z.; Yuan, X.; Yu, Y.; Zhang, Q.; Leong, D. T.; Lee, J. Y.; Xie, J., From Aggregation-Induced Emission of Au(I)–Thiolate Complexes to Ultrabright Au(0)@Au(I)–Thiolate Core–Shell Nanoclusters. *J. Am. Chem. Soc.* **2012,** *134* (40), 16662-16670.
12. Srinivasulu, Y. G.; Goswami, N.; Yao, Q.; Xie, J., High-Yield Synthesis of AIE-Type $Au_{22}(SG)_{18}$ Nanoclusters through Precursor Engineering and Its pH-Dependent Size Transformation. *J. Phys. Chem. C* **2021,** *125* (7), 4066-4076.
13. Xie, J.; Zheng, Y.; Ying, J. Y., Protein-directed synthesis of highly fluorescent gold nanoclusters. *J. Am. Chem. Soc.* **2009,** *131* (3), 888-889.
14. Huang, C. C.; Yang, Z.; Lee, K. H.; Chang, H. T., Synthesis of highly fluorescent gold nanoparticles for sensing Mercury(II). *Angew. Chem.-Int. Edit.* **2007,** *46* (36), 6824-6828.
15. Russier-Antoine, I.; Bertorelle, F.; Hamouda, R.; Rayane, D.; Dugourd, P.; Sanader, Ž.; Bonačić-Koutecký, V.; Brevet, P.-F.; Antoine, R., Tuning Ag_{29} nanocluster light emission from red to blue with one and two-photon excitation. *Nanoscale* **2016,** *8* (5), 2892-2898.
16. AbdulHalim, L. G.; Bootharaju, M. S.; Tang, Q.; Del Gobbo, S.; AbdulHalim, R. G.; Eddaoudi, M.; Jiang, D.-e.; Bakr, O. M., $Ag_{29}(BDT)_{12}(TPP)_4$: A Tetravalent Nanocluster. *J. Am. Chem. Soc.* **2015,** *137* (37), 11970-11975.
17. Veenstra, A. P.; Monzel, L.; Baksi, A.; Czekner, J.; Lebedkin, S.; Schneider, E. K.; Pradeep, T.; Unterreiner, A.-N.; Kappes, M. M., Ultrafast Intersystem Crossing in Isolated $Ag_{29}(BDT)_{12}^{3-}$ Probed by Time-Resolved Pump–Probe Photoelectron Spectroscopy. *J. Phys. Chem. Lett.* **2020,** *11* (7), 2675-2681.
18. Kang, X.; Wang, S.; Zhu, M., Observation of a new type of aggregation-induced emission in nanoclusters. *Chem. Sci.* **2018,** *9* (11), 3062-3068.
19. Soldan, G.; Aljuhani, M. A.; Bootharaju, M. S.; AbdulHalim, L. G.; Parida, M. R.; Emwas, A.-H.; Mohammed, O. F.; Bakr, O. M., Gold Doping of Silver Nanoclusters: A 26-Fold Enhancement in the Luminescence Quantum Yield. *Angew. Chem. Int. Ed.* **2016,** *55* (19), 5749-5753.
20. Khatun, E.; Ghosh, A.; Chakraborty, P.; Singh, P.; Bodiuzzaman, M.; Ganesan, P.; Nataranjan, G.; Ghosh, J.; Pal, S. K.; Pradeep, T., A thirty-fold photoluminescence enhancement induced by secondary ligands in monolayer protected silver clusters. *Nanoscale* **2018,** *10* (42), 20033-20042.
21. Mishra, D.; Lobodin, V.; Zhang, C.; Aldeek, F.; Lochner, E.; Mattoussi, H., Gold-doped silver nanoclusters with enhanced photophysical properties. *Phys. Chem. Chem. Phys.* **2018,** *20* (18), 12992-13007.
22. Zhu, L.; Gharib, M.; Becker, C.; Zeng, Y.; Ziefuß, A. R.; Chen, L.; Alkilany, A. M.; Rehbock, C.; Barcikowski, S.; Parak, W. J.; Chakraborty, I., Synthesis of Fluorescent Silver Nanoclusters: Introducing Bottom-Up and Top-Down Approaches to Nanochemistry in a Single Laboratory Class. *J. Chem. Educ.* **2020,** *97*, 239-243.
23. Udaya Bhaskara Rao, T.; Pradeep, T., Luminescent Ag7 and Ag_8 Clusters by Interfacial Synthesis. *Angew. Chem. Int. Ed.* **2010,** *49* (23), 3925-3929.
24. Zhu, L.; Zeng, Y.; Teubner, M.; Grimm-Lebsanft, B.; Ziefuß, A.; Rehbock, C.; Rübhausen, M.; Barcikowski, S.; Parak, W. J.; Chakraborty, I., Surface Engineering of Gold Nanoclusters Protected with 11-Mercaptoundecanoic Acid for Photoluminescence Sensing. *ACS Appl. Nano Mater.* **2021**, *4* (3), 3197-3203.
25. Chakraborty, I.; Udayabhaskararao, T.; Pradeep, T., High temperature nucleation and growth of glutathione protected~ Ag_{75} clusters. *Chem. Commun.* **2012,** *48* (54), 6788-6790.
26. Chakraborty, I.; Udayabhaskararao, T.; Pradeep, T., Luminescent sub-nanometer clusters for metal ion sensing: A new direction in nanosensors. *J. Hazard. Mater.* **2012,** *211-212*, 396-403.
27. van der Linden, M.; Barendregt, A.; van Bunningen, A. J.; Chin, P. T. K.; Thies-Weesie, D.; de Groot, F. M. F.; Meijerink, A., Characterisation, degradation and regeneration of luminescent Ag_{29} clusters in solution. *Nanoscale* **2016,** *8* (47), 19901-19909.
28. Song, Y.; Murray, R. W., Dynamics and Extent of Ligand Exchange Depend on Electronic Charge of Metal Nanoparticles. *J. Am. Chem. Soc.* **2002,** *124* (24), 7096-7102.
29. Huang, Z.; Ishida, Y.; Narita, K.; Yonezawa, T., Kinetics of Cationic-Ligand-Exchange Reactions in Au_{25} Nanoclusters. *J. Phys. Chem. C* **2018,** *122* (31), 18142-18150.
30. Li, M.-B.; Tian, S.-K.; Wu, Z.; Jin, R., Peeling the Core–Shell Au_{25} Nanocluster by Reverse Ligand-Exchange. *Chem. Mater.* **2016,** *28* (4), 1022-1025.
31. Su, X.; Liu, J., pH-Guided Self-Assembly of Copper Nanoclusters with Aggregation-Induced Emission. *ACS Appl. Mater. Inter.* **2017,** *9* (4), 3902-3910.
32. Chin, P. T.; van der Linden, M.; van Harten, E. J.; Barendregt, A.; Rood, M. T.; Koster, A. J.; van Leeuwen, F. W.; de Mello Donega, C.; Heck, A. J.; Meijerink, A., Enhanced luminescence of Ag nanoclusters via surface modification. *Nanotechnology* **2013,** *24* (7), 075703.
33. Schwans, J. P.; Sunden, F.; Lassila, J. K.; Gonzalez, A.; Tsai, Y.; Herschlag, D., Use of anion–aromatic interactions to position the general base in the ketosteroid isomerase active site. *Proc. Natl. Acad. Sci.* **2013,** *110* (28), 11308-11313.
34. Barraza, R.; Borschel, E. M.; Buback, M., Dimerization of Carboxylic Acids in Solution up to High Pressures and Temperatures. 2. Benzoic Acid. *Zeitschrift für Naturforschung A* **1987,** *42* (4), 406-412.
35. Tsivintzelis, I.; Kontogeorgis, G. M.; Panayiotou, C., Dimerization of Carboxylic Acids: An Equation of State Approach. *J. Phys. Chem. B* **2017,** *121* (9), 2153-2163.

36. Chen, J.; Brooks, C. L.; Scheraga, H. A., Revisiting the Carboxylic Acid Dimers in Aqueous Solution: Interplay of Hydrogen Bonding, Hydrophobic Interactions, and Entropy. *J. Phys. Chem. B* **2008,** *112* (2), 242-249.
37. Yang, T. Q.; Peng, B.; Shan, B. Q.; Zong, Y. X.; Jiang, J. G.; Wu, P.; Zhang, K., Origin of the Photoluminescence of Metal Nanoclusters: From Metal-Centered Emission to Ligand-Centered Emission. *Nanomaterials (Basel)* **2020,** *10* (2).
38. Thanthirige, V. D.; Sinn, E.; Wiederrecht, G. P.; Ramakrishna, G., Unusual Solvent Effects on Optical Properties of Bi-Icosahedral Au_{25} Clusters. *J. Phys. Chem. C* **2017,** *121* (6), 3530-3539.
39. Chevrier, D. M.; Raich, L.; Rovira, C.; Das, A.; Luo, Z.; Yao, Q.; Chatt, A.; Xie, J.; Jin, R.; Akola, J.; Zhang, P., Molecular-Scale Ligand Effects in Small Gold–Thiolate Nanoclusters. *J. Am. Chem. Soc.* **2018,** *140* (45), 15430-15436.
40. Yi, C.; Zheng, H.; Herbert, P. J.; Chen, Y.; Jin, R.; Knappenberger, K. L., Ligand- and Solvent-Dependent Electronic Relaxation Dynamics of $Au_{25}(SR)_{18}^-$ Monolayer-Protected Clusters. *J. Phys. Chem. C* **2017,** *121* (44), 24894-24902.
41. Rettig, W., Charge separation in excited states of decoupled systems—TICT compounds and implications regarding the development of new laser dyes and the primary process of vision and photosynthesis. *Angew. Chem. Int. Ed.* **1986,** *25* (11), 971-988.
42. Lakowicz, J. R., Solvent effects on emission spectra. In *Principles of fluorescence spectroscopy*, Springer: **1999**; 185-210.
43. Chuang, K.-T.; Lin, Y.-W., Microwave-Assisted Formation of Gold Nanoclusters Capped in Bovine Serum Albumin and Exhibiting Red or Blue Emission. *J. Phys. Chem. C* **2017,** *121* (48), 26997-27003.
44. Zhou, C.; Sun, C.; Yu, M.; Qin, Y.; Wang, J.; Kim, M.; Zheng, J., Luminescent Gold Nanoparticles with Mixed Valence States Generated from Dissociation of Polymeric Au(I) Thiolates. *J. Phys. Chem. C* **2010,** *114* (17), 7727-7732.
45. Yam, V. W.-W.; Cheng, E. C.-C., Highlights on the recent advances in gold chemistry—a photophysical perspective. *Chem. Soc. Rev.* **2008,** *37* (9), 1806-1813.
46. Bode, B. M.; Gordon, M. S., MacMolPlt: a graphical user interface for GAMESS. *J. Mol. Graphics Modell.* **1998,** *16* (3), 133-138.
47. Baksi, A.; Schneider, E. K.; Weis, P.; Chakraborty, I.; Fuhr, O.; Lebedkin, S.; Parak, W. J.; Kappes, M. M., Linear Size Contraction of Ligand Protected Ag_{29} Clusters by Substituting Ag with Cu. *ACS Nano* **2020,** *14* (11), 15064-15070.
48. Chakraborty, P.; Baksi, A.; Mudedla, S. K.; Nag, A.; Paramasivam, G.; Subramanian, V.; Pradeep, T., Understanding proton capture and cation-induced dimerization of $[Ag_{29}(BDT)_{12}]^{3-}$ clusters by ion mobility mass spectrometry. *Phys. Chem. Chem. Phys.* **2018,** *20* (11), 7593-7603.
49. van der Linden, M.; van Bunningen, A. J.; Amidani, L.; Bransen, M.; Elnaggar, H.; Glatzel, P.; Meijerink, A.; de Groot, F. M. F., Single Au Atom Doping of Silver Nanoclusters. *ACS Nano* **2018,** *12* (12), 12751-12760.
50. Te Velde, G. t.; Bickelhaupt, F. M.; Baerends, E. J.; Fonseca Guerra, C.; van Gisbergen, S. J.; Snijders, J. G.; Ziegler, T., Chemistry with ADF. *J. Comput. Chem.* **2001,** *22* (9), 931-967.
51. Becke, A. D., Density-functional exchange-energy approximation with correct asymptotic behavior. *Phys. Rev. A* **1988,** *38* (6), 3098.
52. Perdew, J. P., Density-functional approximation for the correlation energy of the inhomogeneous electron gas. *Phys. Rev. B* **1986,** *33* (12), 8822.
53. Lenthe, E. v.; Baerends, E.-J.; Snijders, J. G., Relativistic regular two-component Hamiltonians. *J. Chem. Phys.* **1993,** *99* (6), 4597-4610.
54. van Lenthe, E.; Ehlers, A.; Baerends, E.-J., Geometry optimizations in the zero order regular approximation for relativistic effects. *J. Chem. Phys.* **1999,** *110* (18), 8943-8953.
55. Grimme, S., Density functional theory with London dispersion corrections. *Wiley Interdisciplinary Reviews: Computational Molecular Science* **2011,** *1* (2), 211-228.
56. Osinga, V.; Van Gisbergen, S.; Snijders, J.; Baerends, E., Density functional results for isotropic and anisotropic multipole polarizabilities and C 6, C 7, and C 8 Van der Waals dispersion coefficients for molecules. *J. Chem. Phys.* **1997,** *106* (12), 5091-5101.
57. Rüger, R.; Van Lenthe, E.; Heine, T.; Visscher, L., Tight-binding approximations to time-dependent density functional theory—A fast approach for the calculation of electronically excited states. *J. Chem. Phys.* **2016,** *144* (18), 184103.
58. Seth, M.; Mazur, G.; Ziegler, T., Time-dependent density functional theory gradients in the Amsterdam density functional package: geometry optimizations of spin-flip excitations. *Theor. Chem. Acc.* **2011,** *129* (3-5), 331-342.

Table of Contents (TOC)